CFD Investigation of Dispersion of Airborne Particulate Contaminants in a Raised Floor Data Center

Satyam Saini, Pardeep Shahi, Pratik Bansode, Ashwin Siddarth, Dereje Agonafer
The University of Texas at Arlington
701 S Nedderman Drive
Arlington, Texas
satyam.saini@mavs.uta.edu

Abstract

Modern data center facilities administrators are finding it increasingly difficult to lower the costs incurred in mechanical cooling of their IT equipment. This is especially true for high computing applications like Artificial Intelligence, Bitcoin Mining, Deep Learning, etc. Airside Economization/free air cooling reduces the mechanical cooling costs by using outside air to cool IT equipment under favorable ambient conditions. In this process, administrators risk their equipment to the exposure of fine particulate/gaseous contaminants that might enter the data center facility with the cooling airflow. Literature suggests that the nature of failures caused by particulate contamination is very intermittent which makes the failures tough to predict. While the recommended filters can remove $PM_{10-2.5}$, it's the fine and ultra-fine particulates like DPM (Diesel Particulate Matter), corrosive salts of high ionic content like sulfates and nitrates with low DRH (Deliquescent Relative Humidity) values that are the cause of concern.

The present investigation utilizes a 3-D CFD modeling of particle-laden flow in a rectangular flow domain, imitating the flow through floor tiles as in a raised floor data center. Literature was reviewed to study various numerical models that have been used for simulating particle dispersion and particle deposition in ventilated rooms, air ducts and particle behavior across physical obstructions of various geometries. A Discrete Phase Modeling approach was chosen using ANSYS FLUENT to calculate trajectories of the dispersed contaminants. 6SigmaRoom was used to predict accurate boundary and flow conditions of the fluid flow leaving the floor tiles.

Keywords

CFD, Particle Transport, Data Center, Servers, Contamination

Nomenclature

ACH	Air Change per Hour
CFD	Computational Fluid Dynamics
CBB	Confined Bluff Body
DPM	Diesel Particulate Matter
DRH	Deliquescent Relative Humidity
ISO	International Standards Organization
MERV	Minimum Efficiency Reporting Value
PCB	Printed Circuit Board
RANS	Reynolds Averaged Navier Stokes
Re	Reynolds Number
SIMPLE	Semi Implicit Method for Pressure Linked Equations
SIR	Surface Insulation Resistance

1. Introduction

To cope with rising computation and cloud storage demands, data center proliferation has been increasing unabatedly. Rising computational needs have also increased power densities at the chip level, causing a corresponding spike in the cooling demands. While novel cooling technologies like indirect and direct liquid cooling and immersion-cooling, evaporative cooling [27-29,36,39], have been shown to dissipate high heat fluxes, cloud providers like Google, Microsoft and Facebook have achieved PUE close to 1.1 using free air cooling at ideal locations. [1-3] Still, the majority of the data center administrators refrain from resorting to frees air-cooling methods owing to overhead costs of filters and dehumidification devices installation and the threat of introducing particulate and gaseous contaminants into the data center white space.

The ASHRAE T.C.9.9 subcommittee on Mission Critical Facilities, Data Centers, Technology Spaces and Electronic equipment has defined temperature and humidity ranges to ensure reliable operation of IT equipment [9-14]. They areaccepted by ITE manufacturers and their clients to be as follows: 18°C to 27°C (64.4°F to 80.6°F) dry bulb temperature, 5.5°C to 15°C (41.9°F to 59°F) dew point temperature, and less than 60% relative humidity. This recommended envelope was expanded by ASHRAE Thermal Guidelines for Data Processing Environments 2008, thereby, allowing short excursions into the allowable regions A1-A3, as shown in Figure 1, and an increase in the number of economizer hours. This exposes the IT equipment to the threat of gaseous and particulate contaminants. Two main failure modes associated with IT equipment failure because of surrounding the environment are: electrical open circuits resulting from corrosion of surface mount components due to gaseous contaminants and electrical short circuits due to copper creep corrosion, electrochemical migration and settled hygroscopic matter.

While much has been studied about the failure modes due to the presence of corrosive gases in the data center environment, less attention has been paid to failures because of particulate contaminants owing to the intermittent nature of the failures. 2011 The Gaseous and Particulate Contaminants Guidelines for Data Centers [23] recommends keeping the data centers clean as per ISO Class 8 by the following means of filtration:

- The room air may be continuously filtered with MERV 8 filters, as recommended by ASHRAE Standard 127 (ASHRAE 2007).
- For data centers using airside economizers, the air entering the data center may be filtered with MERV 11 or MERV 13 filters as recommended by ASHRAE (2009b).

The mechanism involved failure due to settled ionic particulate matter is moisture absorption from the surrounding humid air.

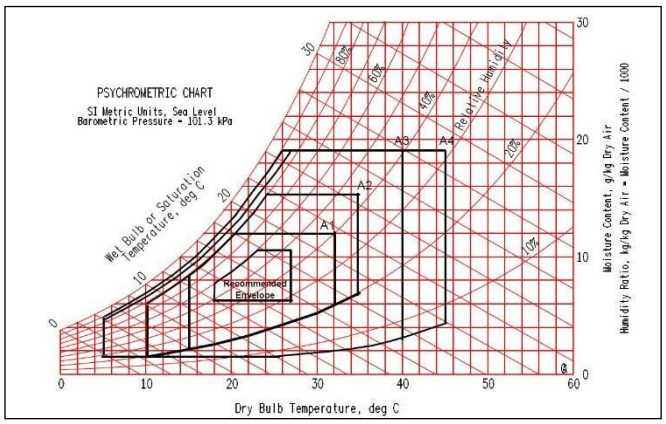

Figure 1: Psychrometric chart for ASHRAE recommended and allowable classes

Such hygroscopic matter forms a conductive aqueous solution above its DRH value, thus, reducing the Surface Insulation Resistance of the PCB and causing short-circuiting of closely spaced PCB features due to ion migration. The above-mentioned concerns point towards a planned effort in addressing these concerns through experimental and numerical studies of the impacts of particulate contamination at the server level.

The present investigation addresses the impacts of particulate contamination in data centers by utilizing a numerical approach to determine the flow patterns of sub-micron-particulate contaminants. Because of a lack of literature on particle transport studies in the data centers, an in-depth literature review was done on particle transport and particle dispersion studies in ducts and ducts with obstructions. Conclusions were made about the dominating forces involved and accurate numerical models to be used by correlating the flow and particle transport characteristics valid for the present investigation. 6SigmaRoom, a commercially available data center CFD code, was used to predict accurate pressure and velocity boundary conditions of the flow through a floor tile in a raised floor data center. The particle transport study was then conducted in ANSYS FLUENT where, for a rectangular flow domain representing volumetric flow rate through a floor tile. A transient Discrete Phase Modeling approach was used to track particle diameters between 1μm-10μm, and realizable k-e model was used to model flow turbulence as per the literature review. Particles were injected in the form of 2-D surface injections at the inlet and a low-pressure boundary condition was used to represent server inlet. Particle tracks and average volume fractions were obtained based on varying particle diameters and particle residence time in the flow.

2. Literature review

Data center contamination because of particulate matter has been addressed in the form of case studies and from a risk assessment point of view, where best practices to mitigate harmful particulates are addressed [30,31]. Existing empirical studies have investigated the failure modes and failure mechanisms, dominated by corrosion studies at PCB level and interconnect level [21,22]. Particle laden flow, in general, has been studied widely for buildings and indoor environments [24-26]. The challenging part in the case of particle-laden flow in data centers is the presence of a multitude of inlets, outlets and varying pressure distribution in the room. To account for the lack of literature and accurate flow models for particle flow in the data centers, the authors constructed a simple model of the flow in a fluid domain, representing flow through a floor tile. The flow and particle transport models were studied from existing literature, as presented below, on particle transport in ducts and 2-D channels with/without obstructions. This enabled the authors to significantly simplify the problem and formulate a set of assumptions that closely matched the flow characteristics in a real-world data center.

An in-depth literature review was done for particle dispersion and deposition studies in ducts and across bluff bodies of various geometries. Several experimental [4,5] and numerical [6-9] investigations have studied the phenomena of particle dispersion in shear flows, where the flow regime is dominated by large vortex formations [18]. Recent examples of particle-laden channel and confined bluff body (CBB) flow can be found in, for example, Breuer and Alletto [10], Mallouppas and vanWachem [11], Sardina, Schlatter, Brandt, Picano, and Casciola [12] and Wang, Manhart, and Zhang [13], while turbulence modification in turbulent particle-laden channel flows can be found in Vreman [14, 19].

The deposition efficiency of liquid particles in 5.03–8.51 mm diameter circular cross-section tubes was investigated by Pui et al. in both turbulent and laminar flows [15]. Particle transport and deposition in vertical and horizontal turbulent square duct flows were studied by Zhang and Ahmadi for different gravity directions [16]. This study implemented Direct Numerical Simulation of the Navier–Stokes equation to provide that particle deposition velocity varies as per the direction of gravity. It was concluded that for horizontal ducts, because of gravity, particle deposition velocity on all four surfaces of the square duct is distinct. Most of the previous works have investigated particle sizes of less than 10μm. However, a study carried out by Zhao and Wu brought something new to the particle size selection [17]. Particle size distribution deposited on the ventilation duct was investigated in a room (4 m x 2.5 m x 3 m) with a typical mechanical ventilation system. The air supply volume rate was 240m^3/hour and the corresponding air change rate was 8 air changes per hour (ACH). The study reported that although the particle diameters smaller than 10 μm are the majorly airborne through the duct, the particles deposited on the duct surface are mostly larger than 10 μm [20].

3. Numerical Method

Particle-laden flow is a common phenomenon for many practical daily indoor and technical applications. CFD enables detailed prediction of complex fluid flows by discretizing complex geometries into smaller regions and numerically solving the desired flow characteristics in these individual discretized regions. Commercially available CFD codes have made it easier to visualize complicated flow phenomena like particle-particle interactions and particle-flow interactions.

Lagrange-Euler approach has been proven to solve multiphase particle-laden flows. This approach uses RANS equations to solve the continuous or carrier phase and the dispersed or particle phase is resolved by Lagrangian tracking. The CFD code was chosen based on its extensive abilities in

resolving particle-particle, particle-flow interactions and accurate mathematical models in simulating turbulence involved in particle flow. As described in ANSYS FLUENT Theory guide [32,33], the continuous phase is calculated using the RANS equations as given below:

$$\nabla . \bar{u} = 0 \tag{1}$$

$$\frac{\partial u}{\partial t} + \rho\,(\bar{u}.\nabla)\bar{u} = -\nabla\bar{p} + \eta\Delta\bar{u} - \nabla.\overline{\tau^{RS}} + \bar{f}_D \tag{2}$$

Where $\bar{u}$ and $\bar{p}$ are the average velocities of continuous (air) and discrete (particle) phase. The second term on the left-hand side in equation (2) represents the Reynolds Stresses which are modeled using the eddy-viscosity approach. In this study, realizable RNG κ-ε model was used to model kinetic energy and turbulent dissipation. Equations (3), (4) and, (5) are solved to obtain the particle force balance and particle trajectories of particles of mass m_p.

$$m_p \frac{d\overrightarrow{u_p}}{dt} = \sum \overline{F_i} \tag{3}$$

$$\sum \overline{F_i} = \overline{F_D} + \overline{F_B} + \overline{F_G} \tag{4}$$

$$m_p \frac{d\overrightarrow{u_p}}{dt} = m_p \frac{\vec{u} - \vec{u}_p}{\tau_r} + m_p \frac{\vec{u}(\rho_p - \rho)}{\rho_p} + \vec{F} \tag{5}$$

The particles were assumed to be smooth and spherical, therefore, spherical drag law was activated, and default values of the coefficients were used for particles greater than 1µm. For sub-micron particles, as explained in theory guide, Stoke Cunningham drag law was used, which is given by equations 6, 7 and 8.

$$\overline{F_D} = \frac{3}{4}\frac{\rho}{\rho_p}\frac{d_p}{m_p} C_D(\vec{u} - \vec{u}_p)|\vec{u} - \vec{u}_p| \tag{6}$$

$$F_D = \frac{18\mu}{d_p^2 \rho C_C} \tag{7}$$

$$C_C = 1 + \frac{2\lambda}{d_p}(1.257 + 0.4) \tag{8}$$

The particle relaxation time was used for predicting particle trajectories using the force balance on the particle in the Lagrangian time frame as given in equation (5). This describes the deacceleration of particles due to the drag force and was solved using equation (9).

$$\tau_r = \frac{\rho_p d_p^2}{18\mu}\frac{24}{C_d Re} \tag{9}$$

Here Re is the relative Reynolds number and is calculated by:

$$Re_p = \frac{\left|\vec{u} - \overrightarrow{u_p}\right|\rho d_p}{\mu} \tag{10}$$

As the particles considered in this study are of small diameter, the torque or particle rotation was not considered. For sub-micron particles, it has been concluded from the literature that their dispersion is dominated by Brownian Force which is calculated using equation (11). The particle lifts for particle diameters greater than 1µm can be solved using equation (12).

$$F_{bi} = \zeta_i \sqrt{\frac{216\rho\nu\sigma T}{\pi\rho_p^2 d_p^5 C_c \Delta t}} \tag{11}$$

$$\vec{F} = m_p \frac{2K v^{\frac{1}{2}} \rho d_{ij}}{\rho_p d_p (d_{lk} d_{kl})^{\frac{1}{4}}}(\vec{u} - \vec{u}_p) \tag{12}$$

The Discrete Random Walk Model or eddy lifetime model can be used to model particle interaction with discrete fluid phase turbulent eddies which are classified by random velocity fluctuations given by u', v', w' and are calculated as given below in equations (13)-(15) where ζ is a normally distributed random number. The value of the RMS (Root Mean Square) fluctuating components on the right-hand side of these equations is calculated by equation (16) using known values of kinetic energy turbulence at each point in the flow.

$$u' = \zeta\sqrt{u'^2} \tag{13}$$

$$v' = \zeta\sqrt{v'^2} \tag{14}$$

$$w' = \zeta\sqrt{w'^2} \tag{15}$$

The characteristic lifetime of an eddy is given by equation (16). The same can be calculated using equation (17) as random variation about T_L, fluid Lagrangian integral time, r is a uniform random number greater than zero and less than 1 and C_L is the integral time scale constant.

$$\tau_e = 2T_L \tag{16}$$

$$\tau_e = -T_L \ln(r) \tag{17}$$

$$T_L = C_L \frac{k}{\epsilon} \tag{18}$$

4. Methodology

After an in-depth literature review of existing literature on particle transport in ducts, a set of assumptions was formulated that would simplify the current model giving near accurate results. A pressure-based solver was used for solving carrier fluid flow and pressure velocity coupling is achieved using the SIMPLE algorithm [38]. Based on the generated flow field, a defined number of particles were injected and were tracked as they traveled through the flow domain.

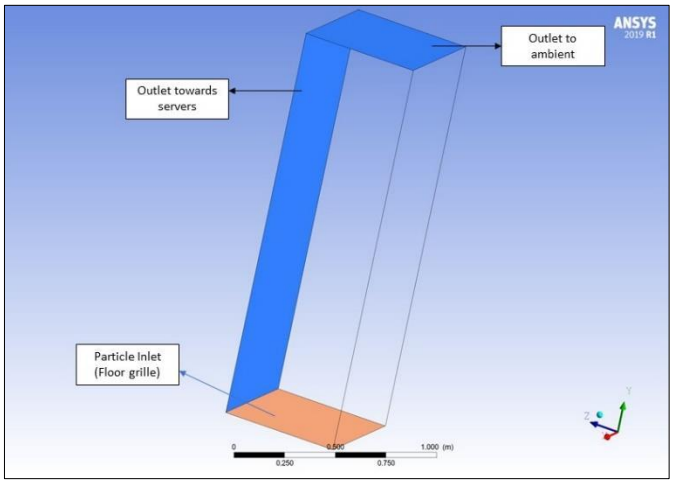

Figure 2: Boundary conditions used in the CFD study

The flow domain was designed in ANSYS DM as a rectangular channel extruded as a fluid representing the flow through a floor tile. Figure 2 shows the set of boundary conditions used in the CFD study, where a 0 Pa gauge pressure boundary condition was used for the outlet to ambient and -0.1 Pa for the outlet towards the servers. The meshing was done using an integrated mesher in the CFD code. As there were no obstructions curvatures within the flow domain, a fine quality mesh was homogenously generated consisting of 747,921 nodes. To visualize accurate boundary conditions, 6SigmaRoom was used to model airflow through floor tiles in a raised floor data center. This was done to realize the effect of neighboring floor tiles on the airflow through any specific tile. A server rack filled with 42 1U servers was modeled in front of a row of five floor tiles with an open area of 29%. 2-D contours of velocity through the floor tiles and pressure contours at the rack inlet were obtained. The obtained values of the velocity and pressure were then used in the CFD code.

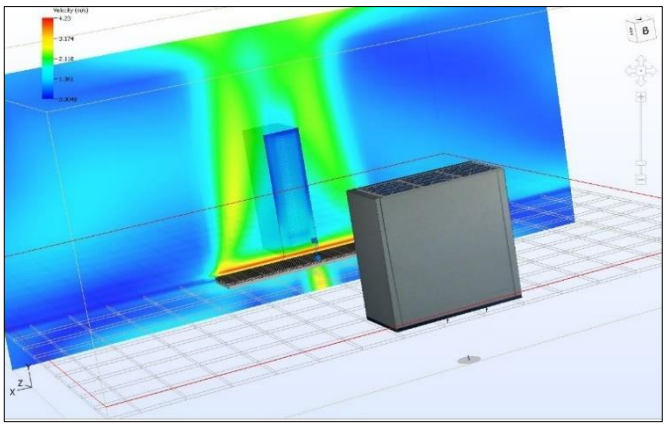

Figure 3: Velocity profile through floor tile in 6SigmaRoom

As seen in Figure 3, a rather constant velocity contour can be seen in front of the server rack with a maximum outlet velocity of 4m/s from the floor tile. As seen from the pressure distribution in the front of the rack in Figure 4, the boundary condition at the outlet towards the servers in FLUENT was given as -0.1 Pa of gauge pressure.

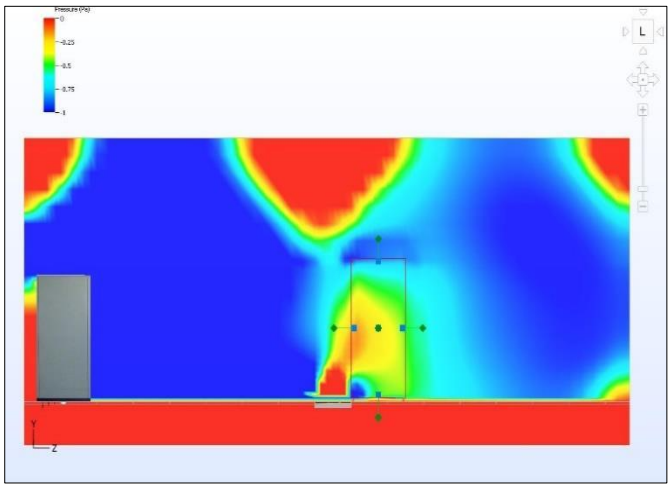

Figure 4: Pressure variation as seen in front of the rack in 6Sigma Room with a minimum pressure of -1 Pa

To validate the particle transport approach used, a validation study was conducted by simulating particle

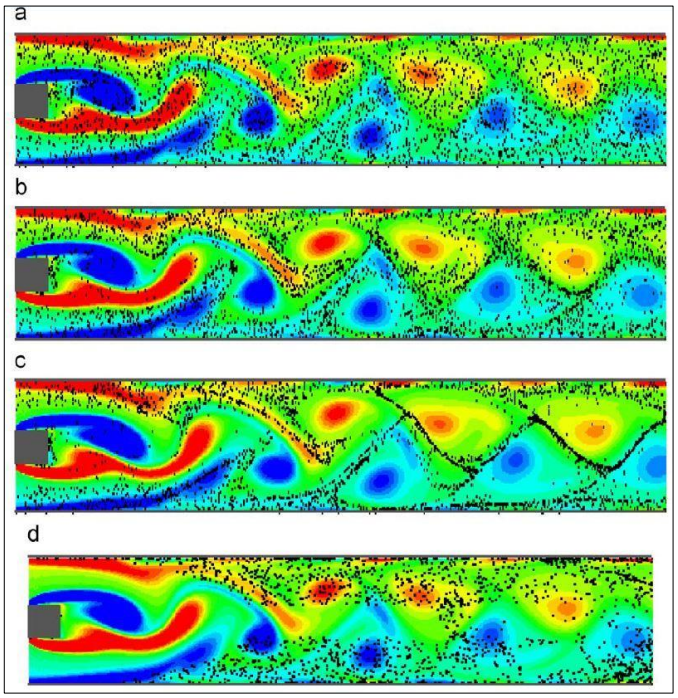

Figure 5: Validation case from the literature review [34]

dispersion across a 2D square cylindrical obstruction in a channel flow as described by Jafari et al [34]. As most of the particle transport studies in the reviewed literature use numerical techniques to model particle transport, it was necessary to determine if the models available in the CFD code could give near similar results to numerical exact solutions. The reviewed study numerically modeled particle transport and

deposition by correlating the flow Stokes number for laminar flow. Similar mathematical models for forces and flow were activated in ANSYS and a transient simulation was run with a time step of 0.01 seconds for 1000 time steps. This allowed the flow to sufficiently fill the entire domain and aided in visualizing the vortex shedding across the bluff body as seen in Figure 5. This study concluded that particle dispersion is dominated by Brownian motion for sub-micron particles and by inertia forces for particle sizes of larger diameters.

The particle dispersion is also selectively distributed based on particle size. Smaller particles were unaffected due to the presence of the vortices, as can be seen in Figure 5. While the heavier particles are distributed on the periphery of the shed vortices. This is because inertial particles tend to move towards low vorticity regions because of the vortex generated centrifugal forces. Using the same design parameters and geometries, particle dispersion was obtained in the CFD code. The comparison of both the reviewed study and current study can be seen below, and a similar pattern is observed in present simulations as seen below in Figure 6.

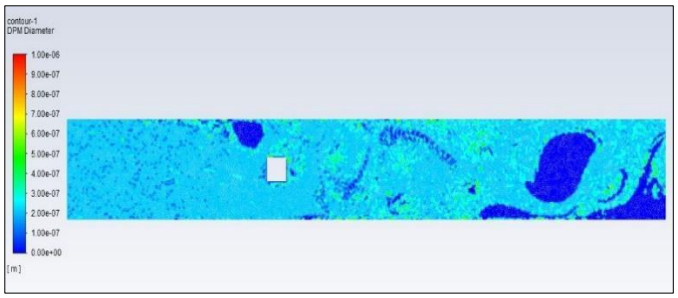

Figure 6: Particle traces as obtained for validation case

5. Results and Discussion

The final flow domain was imported to the CFD code and appropriate flow models and boundary conditions were activated as explained in Section 3 and Section 4. The particles were injected as surface injections where particles were then released from each facet of the surface. Here, the facet value of a variable is defined as the computed arithmetic average of the adjacent cell values of the variable. A total flow rate of 1e-04 kg/m^3 was used so that a sufficient number of particles can be generated and tracked. The maximum, minimum and mean diameters of the injections were specified

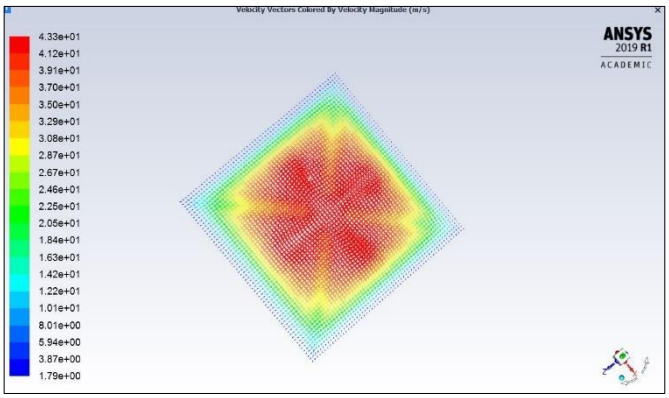

Figure 7: Velocity vectors of air at the outlet for base flow simulation

for size distribution. The particle properties were selected using anthracite (ρ=1550kg/m^3) as an inert particle from the software material library and relevant force balance laws were activated. Two-way coupling was used in which the continuous flow field was solved first, after which the discrete phase trajectories are calculated. After this, the continuous phase was solved again based on interphase momentum exchange (as no heat and mass transfer is considered in this study) and discrete phase trajectories were then recalculated for a modified flow field. This process was repeated until a converged solution was obtained. For the current study, a DPM iteration interval of 10 was selected, which means that a discrete phase iteration was performed every tenth continuous phase iteration. A time step size of 0.1 seconds was chosen with a total number of iterations equal to 100 and maximum iterations per time step equal to 10.

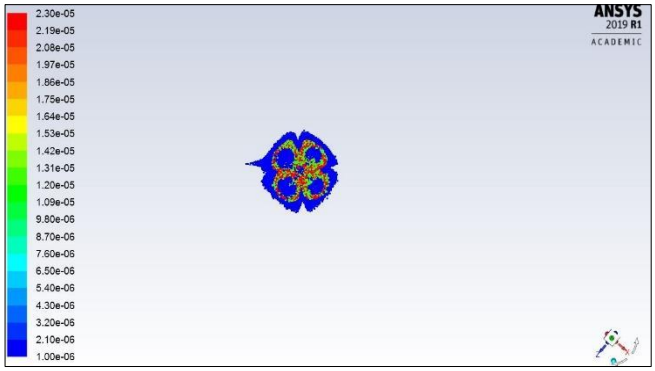

Figure 8: Particle concentration contour for various diameters

Multiple simulations were run after completing the validation case. The first case simulated in the present study was that of a rectangular channel with all four sides of the channel in a symmetry boundary condition. This was done to validate the approach that without any influence of gravity, all the particles must follow the flow streamlines of air/continuous fluid. Figure 7 shows the velocity profile of the flow as seen at the domain outlet. Comparing the velocity contour to the particle concentration, as seen in Figure 8, it can be concluded that the assumption made about particle following the flow streamlines holds. Also, from the knowledge of fluid dynamics, for a flow in a rectangular duct, the maximum flow velocity should occur at the center of the duct.

A similar flow and selective concentration pattern were observed for the particles, in this case, irrespective of their diameters. Unlike succeeding simulations, the effects of buoyancy and Brownian motion were ignored for the base simulation. Another base simulation with a particle diameter less than 1µm was also performed which showed the same flow pattern and was, therefore, not included in the results to avoid the repeated presentation of similar patterns.

The next and final set of simulations was performed by defining a second low-pressure outlet in the flow domain depicting the floor tile side facing the rack inlet. The value of the pressure was chosen from 6SigmaRoom by populating a

rack with 42 1U servers and plotting a pressure contour on the

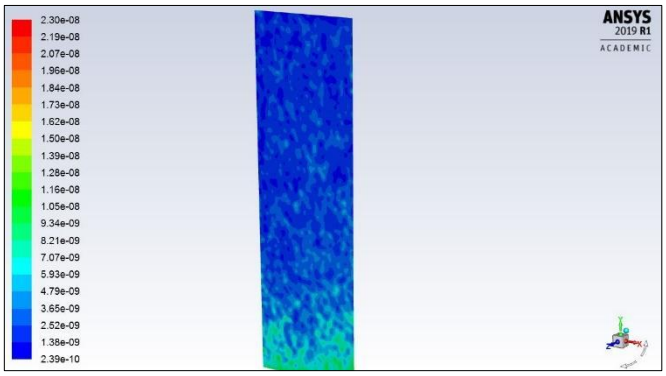

Figure 9: Particle concentration distribution on server side for low-density particles

server inlets. It was assumed that all the servers operated under a constant load, hence creating a constant pressure drop across the width of the rack. The other three sides of the flow domain were given a symmetry boundary condition. Physically, the symmetry boundary condition, in this case, can be interpreted as a floor tile present at the center of a cabinet row with no effect on its airflow from any of the neighboring tiles. Unlike the previous case, the effects of particle buoyancy and Brownian motion were also considered. Figure 10 shows the instantaneous distribution of particles based on particle diameters.

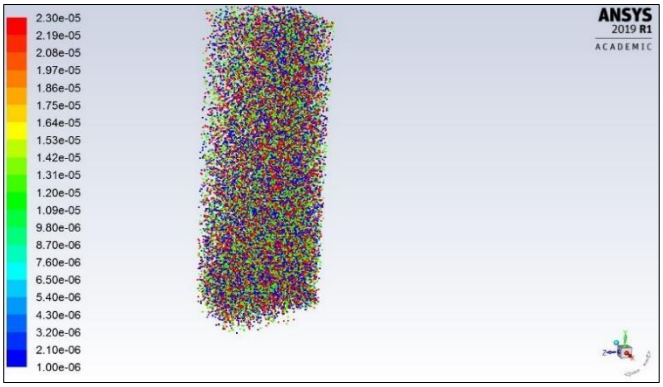

Figure 10: Real time Particle diameter distribution in flow domain after complete simulation

Figure 9 shows the concentration distribution of low-density particles as observed at the flow domain side facing the server inlets. Comparing this to Figure 11, the distribution of particles is more pronounced at the bottom and top ends of the

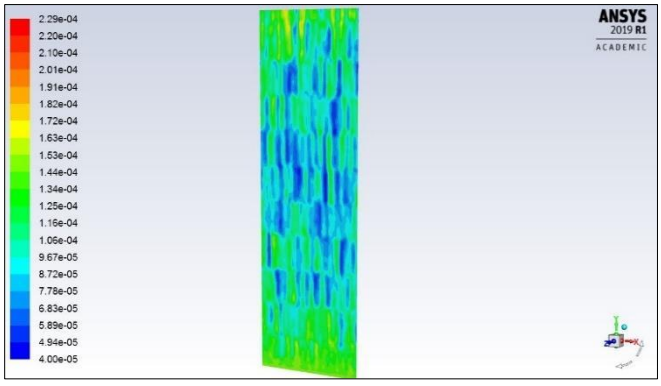

Figure 11: Particle concentration of dense particles on the server inlet side

flow domain faces. Finally, the density of the particles was increased to 8800 kg/m^3 to see how a large variation in density of the inert particles will affect the particle tracks obtained under the same boundary conditions.

Figure 11 and Figure 12 show overall particle concentration by total mass and concentration variation by diameters on the domain face towards the rack inlet respectively. Most of the particle mass was retained at the bottom of the domain and escaped through the outlet facing the servers. The particle diameter distribution at the final time step shows that most of the particles that escaped the outlet facing the servers were of diameters less than the mean diameter considered in this simulation. The inequality in the parentheses represents mean diameter in the simulation bounded by minimum and maximum diameters (1e-07µm <5e-07 µm <1e-06 µm).

Property	Server side	Top outlet
Mass transfer	1.77e-04 kg	7e-04 kg
No. of particles escaped	6.4e+05	2.6e+08
Max. time before escaping	2.19 sec	2.15 sec

Table 1: Particle summary for low-density particles

The bulk distribution within the fluid domain of particle diameters was observed to be slightly different than that of lighter particles. This was observed from the fact that a greater number of particles escaped out from the inlet itself when compared to the particles of low density.

Property	Server side	Top outlet
Mass transfer	1.77e-04 kg	7e-04 kg
No. of particles escaped	1.6e+06	1.8e+06
Max. time before escaping	2.1 sec	1.83 sec

Table 2: Particle summary for high-density particles

Since a lot of elements in the flow domain were reported by the solver having reverse flow because of a low-pressure outlet, as concluded from the validation case, the heavier particles can be trapped in their vicinity and stay in the flow domain for longer times. Particle summary was obtained in post-processing which showed that a total of 3.4e12 particles were ejected from the floor tile for 10 seconds for low-density particles. Table 1 shows the number of particles and mass transferred from the two outlets considered in the flow domain. The total mass and the number of particles escaped from the top outlet is almost four times greater than the outlet facing the servers. This means that less than 10e-07 of the total particles injected and tracked by the solver went towards the IT equipment. Although this number might seem small, as the literature suggests the failures related to particulates are intermittent and happen after sufficient particulate

accumulation and favorable environmental conditions. For high-density particles, the total particle count injected in the flow domain was around 1.9e+11. The fraction of particles escaping towards the server side was an order of magnitude more than that obtained for lighter particles. Also, the total number of particles escaping both the outlets were similar.

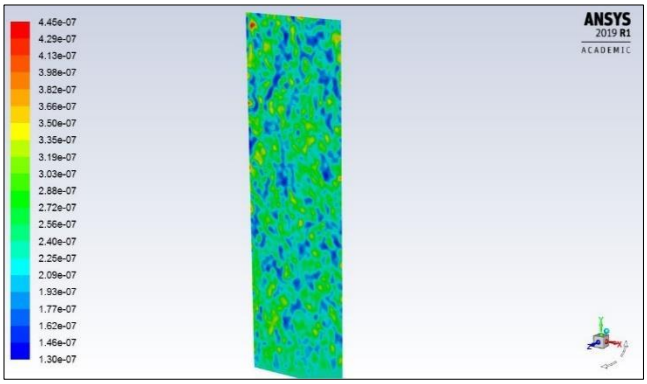

Figure 12: Particle diameter distribution at the side facing server inlets for high-density particles

6. Conclusions

Particle transport of particulate contaminants was studied for a simplified model of a raised floor data center using CFD. Particle distribution was obtained for various boundary conditions within the flow domain and two different particle densities. The approach was validated as per existing particle dispersion studies in the literature. It was observed that particle sizes or particle mass is the dominant factor that dictates particle dispersion. For lighter or lower diameter particles, the dispersion was rather random. Also, the particle concentration plots obtained show that particle deposition will be more pronounced around the bottom servers due to low-pressure regions. This observation might need actual experimental validation, where either outflow or pressure variation can be measured at the rack level in an actual data center. The particle escape regions were inferred to be located towards the bottom of the flow domain, implying that the maximum particle concentration or deposition should be found in the servers located at the bottom of the flow domain.

In a real flow inside IT equipment, when the vortices formed due to impedance inside the server eventually lose their energy, the particles carried by them will be deposited at that location. For servers, where the flow is enclosed and is generally incident on multiple obstructions, it can be predicted that the stagnation points of the flow on these obstructions will be most vulnerable to particle deposition. It can be further extrapolated that if some of these particles are ionic in nature, there can be a high probability of equipment failure due to short-circuiting. Further simulations of particle flow within the server will give a better interpretation of the deposition and dispersion phenomenon within the server. Various raised floor data center cooling strategies and local airflow delivery methods through floor tiles [37] will also affect the particle distribution. This necessitates the requirement of further detailed simulations of the floor tile itself to get a better idea of special distribution and dispersion of the particulate contaminants. Particle distribution will also be dependent on particle shape based on variation in drag and lift forces [40] which should also be taken into account for future studies.

7. Future Work

This study is preliminary work in conducting a detailed study of the particle-laden airflow through the server rack as well as individual IT equipment. A detailed model of the combined floor tile and server rack will be created by experimentally determining the pressure drops across the server rack and inlet and outlet velocities. The effect of changes in particle particulate characteristics like particle density, diameters, and particle coagulation will be seen. The objectives of these subsequent studies are to determine the percentage deposition occurring inside the server and using CFD, predicting the locations of these depositions based on flow characteristics inside the server. User-defined functions can be compiled and imported into the CFD solver to study particle deposition which is directly related to particle's Stokes number.

Acknowledgments

This work is supported by NSF I/UCRC in Energy-Smart Electronic Systems (ES2). The authors would also like to extend special gratitude towards Mark Seymour and Kourosh Nemati of Future Facilities for their guidance and feedback throughout the project.

References

1. https://www.opencompute.org/blog/cooling-an-ocp-data-center-in-a-hot-and-humid-climate
2. Google. Efficiency: How We Do It, 2014
3. Microsoft. Microsoft Shares Video Tour of its Cloud Datacenters,2011
4. Longmire, E. K., and Eaton, J. K. (1992). Structure of a Particle-Laden Round Jet, *J. Fluid Mech.* 236:217–257.
5. Lazaro, B. J., and Lasheras, J. C. (1992). Particle Dispersion in the Developing Free Shear Layer, Part 1—Unforced Flow, *J. Fluid Mech.* 235:143–178.
6. Crowe, C. T., Chung, J. N., and Trout, T. R. (1988). Particle Mixing in Free Shear Flows, *Progress in Energy and Combustion Science* 14:171–194.
7. Uthuppan, J., Aggarwal, S. K., Grinstein, F. F., and Kailasanath, K. (1994). Particle Dispersion in a Transitional Axisymmetric Jet: A Numerical Simulation, *AIAA J.* 32:2004–2014.
8. Aggarwal, S. K. (1994). Relationship Between the Stokes Number and Intrinsic Frequencies in Particle-Laden Flows, *AIAA J.* 32:1322–1325.
9. Chang, E., and Kailasanath, K. (1996). Simulation of Dynamics in a Confined Shear Flow, *AIAA J.* 34:1160–1166
10. Alletto, M., & Breuer, M. (2012). One-way, two-way and four-way coupled LES predictions of a particle-laden turbulent flow at high mass loading downstream of a confined bluff body. *International Journal of Multiphase Flow*, *45*, 70–90.
11. van Vliet, E., Singh, M., Schoonenberg,W., van Oord, J., van der Plas,D., & Deen, N. (2013). *Development and validation of Lagrangian-Eulerian multi-phase model for simulating the argon stirred steel flow in a ladle with slag*. Proceedings of the 5th International Conference on

Modelling and Simulation of Metallurgical Processes in Steelmaking, STEELSIM. Ostrava, Czech Republic.

12. Sardina, G., Schlatter, P., Brandt, L. P., & Casciola, C. (2012). Wall accumulation and spatial localization in particle-laden wall flows. *Journal of Fluid Mechanics*, *699*, 50–78.
13. Wang, B., Manhart, M., & Zhang, H. (2011). Analysis of inertial particle drift dispersion by direct numerical simulation of two-phase wall-bounded turbulent flows. *Engineering Applications of Computational Fluid Mechanics*, *5*(3), 341–348.
14. Vreman, A. (2015). Turbulence attenuation in particle-laden flow in smooth and rough channels. *Journal of Fluid Mechanics*, *773*, 103–136
15. Pui DYH, Romay-Novas F, Liu BYH. Experimental study of particle deposition in bends of circular cross-section. Aerosol Sci Technol 1997;7:301–15
16. Zhang H, Ahmadi G. Aerosol particle transport and deposition in vertical and horizontal turbulent duct flows. J Fluid Mech 2000;406:55–80.
17. Zhao Bin, Wu Jun. Modeling particle fate in ventilation system—Part II: Case study. Build Environ 2009;44:612–20.
18. D. J. Brandon & S. K. Aggarwal (2001) A Numerical Investigation of Particle Deposition on a Square Cylinder Placed in a Channel Flow, Aerosol Science & Technology, 34:4, 340-352
19. Franziska Greifzu, Christoph Kratzsch, Thomas Forgber, Friederike Lindner & Rüdiger Schwarze (2016) Assessment of particle-tracking models for dispersed particle-laden flows implemented in OpenFOAM and ANSYS FLUENT, Engineering Applications of Computational Fluid Mechanics, 10:1, 30-43, DOI: 10.1080/19942060.2015.1104266
20. Gao, R., and Li, A. (2012). Dust Deposition in Ventilation and Air-Conditioning Duct Bend Flows. *Energy Convers. Manage.*, 55:49–59
21. Jimil M. Shah, "Characterizing contamination to expand ASHRAE envelope in airside economization and thermal and reliability in immersion cooling of data centers", PhD dissertation, The University of Texas at Arlington, May 2018
22. Jimil M. Shah, "Reliability challenges in airside economization and oil immersion cooling", UTA-THESIS, 2016-05-16, Shah, Jimil Manojbhai, 0000-0003-2297-7413.
21. Prabjit Singh, Levente Klein, Dereje Agonafer, Jimil M. Shah and Kanan D. Pujara, "Effect of Relative Humidity, Temperature and Gaseous and Particulate Contaminations on ITE Reliability, DOI: 10.1115/IPACK2015-48176, ASME InterPACK 2015, San Francisco, CA.
22. Shah, Jimil & Awe, Oluwaseun & Gebrehiwot, Betsegaw & Agonafer, Dereje & Singh, P & Kannan Mestex, Naveen & Kaler Mestex, Mike. (2017). Qualitative Study of Cumulative Corrosion Damage of ITE in a Data Center Utilizing Air-side Economizer Operating in Recommended and Expanded ASHRAE Envelope. Journal of Electronic Packaging. 139. 021002. 10.1115/1.4036363
23. ASHARE. 2011. 2011 Gaseous and Particulate Guidelines for Data Centers, Atlanta, GA, USA.
24. Seymour, M.J., A. A. M. A., and Jiang, J., 2000. "Cfd based airflow modelling to investigate the effectiveness of control methods intended to prevent the transmission of airborne organisms". Air Distribution in Rooms, (ROOMVENT 2000).
25. Jones, P., and Whittle, G., 1992. "Computational fluid dynamics for building air flow prediction- current status and capabilities". Building and Environment, 27(3), pp. 321–338.
26. Chen, Q., and Zhang, Z., 2005. "Prediction of particle transport in enclosed environment". China Particuology, 3(6), pp. 364–372.
27. Jimil M. Shah, Chinmay Bhatt, Pranavi Rachamreddy, Ravya Dandamudi, Satyam Saini, Dereje Agonafer, 2019, "Computational Form Factor Study of a 3rd Generation Open Compute Server for Single-Phase Immersion Cooling," ASME Conference Paper No. IPACK2019-6602
28. Dhruvkumar Gandhi, Uschas Chowdhury, Tushar Chauhan, Pratik Bansode, Satyam Saini, Jimil M. Shah and Dereje Agonafer, 2019, "Computational analysis for thermal optimization of server for single phase immersion cooling", ASME Conference Paper No. IPACK2019-6587
29. Pravin A Shinde, Pratik V Bansode, Satyam Saini, Rajesh Kasukurthy, Tushar Chauhan, Jimil M Shah and Dereje Agonafer, 2019, "Experimental analysis for optimization of thermal performance of a server in single phase immersion cooling", ASME Conference Paper No. IPACK2019-6590
30. Jimil M. Shah, Roshan Anand, Satyam Saini, Rawhan Cyriac, Dereje Agonafer, Prabjit Singh, Mike Kaler, 2019, "Development of A Technique to Measure Deliquescent Relative Humidity of Particulate Contaminants and Determination of the Operating Relative Humidity of a Data Center, ASME Conference Paper No. IPACK2019-6601
31. Gautham Thirunavakkarasu, Satyam Saini, Jimil Shah, Dereje Agonafer,2018, **"**Airflow pattern and path flow simulation of airborne particulate contaminants in a high-density Data Center utilizing Airside Economization", ASME Conference Paper No. IPACK2018-8436
32. *ANSYS® ANSYS FLUENT Theory Guide, Chapter 16, Release 2019 R1*
33. *ANSYS® ANSYS FLUENT User's Guide, Chapter24, Release 2019 R1*
34. Jafari, Saeed & Salmanzadeh, Mazyar & Rahnama, Mohammad & Ahmadi, Goodarz. (2010). Investigation of particle dispersion and deposition in a channel with a square cylinder obstruction using the lattice Boltzmann method. Journal of Aerosol Science. 41. 198-206. 10.1016/j.jaerosci.2009.10.005.
35. Patankar, S. V., & Spalding, D. B. (1972). A calculation procedure for heat, mass and momentum transfer in threedimensional parabolic flows. *International Journal of Heat and Mass Transfer*, *15*, 1787–1806.
36. Dakshinamurthy, H. N., Siddarth, A., Guhe, A., Kasukurthy, R., Hoverson, J., & Agonafer, D. (2019, January). Accelerated Degradation Testing of Rigid Wet Cooling Media to Analyse the Impact of Calcium Scaling.

In *ASME 2018 International Mechanical Engineering Congress and Exposition*. American Society of Mechanical Engineers Digital Collection.

37. Mohsenian, G., Khalili, S., & Sammakia, B. (2019, May). A Design Methodology for Controlling Local Airflow Delivery in Data Centers Using Air Dampers. In *2019 18th IEEE Intersociety Conference on Thermal and Thermomechanical Phenomena in Electronic Systems (ITherm)* (pp. 905-911). IEEE.
38. Patankar, S. V., & Spalding, D. B. (1972). A calculation procedure for heat, mass and momentum transfer in threedimensional parabolic flows. *International Journal of Heat and Mass Transfer*, *15*, 1787–1806
39. Kumar, A., Shahi, P., & Saha, S. K. Experimental Study of Latent Heat Thermal Energy Storage System for Medium Temperature Solar Applications.
40. Sarker, M. R. H., Chowdhury, A. R., & Love, N. (2017). Prediction of gas–solid bed hydrodynamics using an improved drag correlation for nonspherical particles. *Proceedings of the Institution of Mechanical Engineers, Part C: Journal of Mechanical Engineering Science*, *231*(10), 1826-1838.